Korean J. Chem. Eng., 37(8), 1360-1364 (2020)
DOI: 10.1007/s11814-020-0586-2

pISSN: 0256-1115
eISSN: 1975-7220

Surface engineering of Pd-based nanoparticles by gas treatment for oxygen reduction reaction

A. Anto Jeffery[*,‡], Sang-Young Lee[,‡], Jiho Min[*], Youngjin Kim[*], Seunghyun Lee[*], Jin Hee Lee[***], Namgee Jung[*,†], and Sung Jong Yoo[****,*****,******,†]**

*Graduate School of Energy Science and Technology (GEST), Chungnam National University, 99 Daehak-ro, Yuseong-gu, Daejeon 34134, Korea
**The Environment Technology Institute, Research Division, Coway R&D Center, 1 Guanak-ro, Gwanak-gu, Seoul 08826, Korea
***Center for Environment & Sustainable Resources, Korea Research Institute of Chemical Technology, Daejeon 34114, Korea
****Center for Hydrogen·Fuel Cell Research, Korea Institute of Science and Technology (KIST), Seoul 02792, Korea
*****Division of Energy & Environment Technology, KIST School, University of Science and Technology (UST), Seoul 02792, Korea
******KHU-KIST Department of Converging Science and Technology, Kyung Hee University, Seoul 02447, Korea
(*Received 15 March 2020 • Revised 10 May 2020 • Accepted 20 May 2020*)

Abstract−In many catalyst systems, including fuel cell applications, control of the catalyst surface composition is important for improving activity since catalytic reactions occur only at the surface. However, it is very difficult to modify the surface composition without changing the morphology of metal nanoparticles. Herein, carbon-supported Pd_3Au_1 nanoparticles with uniform size and distribution are fabricated by *tert*-butylamine reduction method. Pd or Au surface segregation is induced by simply heating as-prepared Pd_3Au_1 nanoparticles under CO or Ar atmosphere, respectively. Especially, CO-induced Pd surface segregation allows the alloy nanoparticles to have a Pd-rich surface, which is attributed to the strong CO binding energy of Pd. To demonstrate the change in surface composition of Pd_3Au_1 alloy catalyst with the annealing gas species, the oxygen reduction reaction performance is investigated and consequently, Pd_3Au_1 catalyst with the highest number of surface Pd atoms indicates excellent catalytic activity. Therefore, the present work provides insights into the development of metal-based alloys with optimum structures and surface compositions for various catalytic systems.

Keywords: CO-induced Surface Segregation, Surface Composition, Metal Alloy, Catalyst, Oxygen Reduction Reaction

INTRODUCTION

Proton exchange membrane fuel cells (PEMFCs) are one of the most promising clean and sustainable energy systems to resolve numerous energy-related crises with benefits of low temperature operation, high conversion efficiency, high energy density, and environmentally benign products [1-3]. However, in PEMFCs, the oxygen reduction reaction (ORR) at cathode is sluggish and requires the use of expensive Pt and its alloy materials, which hinders their commercialization [4]. Therefore, tremendous researches have been carried out to explore and develop Pt-free or non-noble metal catalysts for efficient ORR [5,6]. Pd has been known as an important transition metal with high catalytic activity, earth-abundant, less expensive, and suitable for the ORR [5,7-9]. However, Pd catalyst shows relatively low activity and poor stability compared to Pt under dynamic electrochemical conditions. Accordingly, Pd has been alloyed with other transition metals (M=Fe, Co, Ni, Au, Cu, etc.) to improve the ORR activity of Pd catalyst, resulting in interesting electrochemical properties [2,10-14].

Alloying two metal elements provides two important effects, such as ensemble and ligand effects [15,16]. While the ensemble effect is induced by unique geometric configurations, the ligand effect is the result of electronic interaction between two metals [15-17]. However, the two effects can contribute to improving the catalytic activity simultaneously due to the combination of two different metals. Based on previous studies on PdAu alloy catalysts with different structures [2,10,18-21], it is well known that the catalytic properties of PdAu alloys depend strongly on shape, size, and surface composition [22,23]. Although several strategies for synthesis of PdAu alloy with diverse structures have been developed, fine control of the surface composition and particle size of PdAu alloy nanoparticles with increased number of active sites is still challenging.

In previous studies, several researchers demonstrated the synthesis and potential applications of various PdAu alloy nanostructures with controlled surface composition, size, and structure. For example, Yin et al. developed the synthesis of monodispersed bimetallic PdAu nanoparticles through an emulsion-assisted synthetic strategy using metal precursors and surfactants in ethylene glycol (EG) solution. The bimetallic $Pd_{31}Au_{70}$ nanoparticles with low Pd

†To whom correspondence should be addressed.
E-mail: njung@cnu.ac.kr, ysj@kist.re.kr
‡These authors contributed equally to this work.

content showed superior electrocatalytic for methanol oxidation reaction (MOR) compared to Pd and Pt catalysts, demonstrating that the synthesis method is an effective strategy to design Pd-rich shell and Au-rich core structure [24]. Recently, Kumar et al. reported an interesting result on the systematic control of $Pd_{20-x}Au_x$ nanoparticles supported on N-doped graphene by one-pot polyol method. The electronic interaction among Pd, Au, and N-doped graphene and their synergistic effect contributed to enhanced electrocatalytic activity and stability toward MOR and alleviated the CO poisoning effect [19]. Alternatively, Jiao et al. proposed an effective approach to tune the surface properties of PdAu hollow nanospheres by one-pot template method using cobalt nanoparticles as a sacrificial substrate [25]. As a result, the PdAu hollow nanospheres showed much higher ORR activity than a commercial Pt/C catalyst, which was attributed mainly to the strain effect that makes the adsorption strength of oxygen-containing species appropriate.

Here, considering the multifunctional ability of bimetallic PdAu alloy nanostructures and their tunable surface property, a facile strategy to increase the number of active sites in carbon-supported Pd_3Au_1 nanoparticles (Pd_3Au_1/C) through heat treatments under different gas atmospheres is proposed. It is clearly confirmed that the surface composition of Pd and Au in Pd_3Au_1/C catalyst can be tuned without severe particle agglomeration by simply changing the gas atmospheres (Ar or CO) during the heat treatment. Interestingly, when the ORR performance of the surface-controlled Pd_3Au_1/C catalysts is evaluated, they show totally different catalytic activity depending on the surface composition of Pd and Au. The proposed surface tuning method will provide insights into the development of alloy catalysts useful for various catalyst systems as well as electrochemical applications.

EXPERIMENTAL

1. Materials

The entire chemicals purchased were used without any further purification. Palladium(II) acetylacetonate ($Pd(C_5H_7O_2)_2$, 99%), Gold(III) chloride trihydrate ($HAuCl_4 \cdot 3H_2O$, ≥99.9%), oleylamine ($C_{18}H_{35}NH_2$, 70%), anhydrous ethanol (≥99.5%), and borane tert-butylamine ($(CH_3)_3CNH_2 \cdot BH_3$) were purchased from Aldrich.

2. Synthesis

Carbon-supported Pd_3Au_1 nanoparticle catalysts (20 wt% metal loading, 3 : 1 molar ratio Pd : Au) were prepared by *tert*-butylamine reduction method in anhydrous ethanol at room temperature. 0.1 g of carbon black (Vulcan XC-72) was dispersed in anhydrous ethanol (100 ml) through ultrasonication. Meanwhile, oleylamine (3.039 mmol) was added to the suspension and allowed to sonicate for 1 h. Afterwards, Pd(II) acetylacetonate (0.145 mmol), Au(III) chloride trihydrate (0.048 mmol), and borane *tert*-butylamine (1.937 mmol) were dissolved in anhydrous ethanol of different quantities (80, 20, and 20 mL, respectively). To the dispersed carbon black suspension, metal precursors and reducing agent were quickly added in the order Au, Pd, and borane *tert*-butylamine at an interval time of 30 min and the mixture was stirred for 24 h. After 24 h, the slurry was vacuum filtered fitted with a membrane filter, washed with copious amount of ethanol and dried in vacuum oven. To remove surfactant (oleylamine) impurities on catalyst surface, the samples were annealed in air (200 sccm) for 1 h at 200 °C in a tubular furnace (Pd_3Au_1-ASP). To achieve surface segregation of Pd or Au (Pd_3Au_1-Ar or Pd_3Au_1-CO), the as-prepared samples were heated under Ar or CO (200 sccm) for 1 h at 200 °C, whereas the reverse surface segregation (Pd_3Au_1-(CO-Ar)) was achieved by heating the CO-treated sample under Ar atmosphere (200 sccm) for 1 h at 200 °C again. The heat treatment procedure involved heating the catalysts from room temperature to 200 °C (10 °C/min) under N_2 atmosphere (200 sccm) and maintaining N_2 atmosphere (200 sccm) when the elevated temperature is cooled to room temperature before and after the main heat treatment at 200 °C, respectively.

3. Characterization

All the synthesized samples were analyzed by recording X-ray diffraction (XRD) patterns using Rigaku D/MAX 2500 diffractometer equipped with a Cu Kα X-ray source (λ=1.5401 Å). Transmission electron microscopy (TEM) images (Philips CM30) were recorded to confirm particle size and distribution of Pd_3Au_1 electrocatalysts. X-ray photoelectron spectroscopy (XPS) measurements were carried out on PHI-5000 Versa Probe (Ulvac-PHI) to analyze Pd 3d and Au 4f core level regions. The XPS binding energies were calibrated by using a C 1s value of 284.6 eV. Peak fitting was performed by using XPS 4.1 software.

4. Electrochemical Measurements

All electrochemical measurements (Autolab 302N potentiostat) involved using a standard three-electrode electrochemical cell composed of glassy carbon (GC) rotating disk electrode (5 mm diameter, geometric area= 0.196 cm^2), Pt wire, and a saturated calomel electrode as the working, counter and reference electrodes, respectively. The catalyst ink was prepared by dispersing 10 mg of catalyst in 5 wt% Nafion solution (0.1 mL, Aldrich) and 2-propanol (1 mL) for few minutes until homogeneous ink was obtained. A drop of prepared catalyst ink (total metal loading= 44.86 μg cm^2) was drop casted on a GC electrode and then dried at room temperature. Cyclic voltammetry (CV) measurements were carried out between 0.05 to 1.05 V_{RHE} ranges with a scan rate of 20 mV s^{-1} in Ar-purged 0.1 M $HClO_4$ (perchloric acid, ACS reagent, 70%, Aldrich) solution. ORR measurements were carried out at potential range from 0.05 to 1.05 V_{RHE} at a scan rate of 5 mV s^{-1} under a constant rotation speed of 1,600 rpm in O_2-saturated 0.1 M $HClO_4$ solution.

RESULTS AND DISCUSSION

The schematic diagram of the surface rearrangement of Pd_3Au_1 nanoparticles by different gas atmospheres is displayed in Fig. 1. When Pd_3Au_1-ASP as a starting material was treated in Ar, Pd_3Au_1-Ar catalyst with Au-rich surface was produced due to strong Au surface segregation. This result is attributed to lower surface free energy of Au (1.41 J m^{-2}) than that of Pd (2.04 J m^{-2}) [26,27]. Whereas, Pd segregation predominates under CO gas atmosphere since the CO binding energy on Pd (−2.01 eV) is ~6 times higher than that on Au (−0.35 eV) [28,29]. Concurrently, when CO-induced Pd segregated nanoparticle was further subjected to the Ar heat treatment, Au atoms are segregated into the surface again, which implies that Pd or Au surface enrichment on the PdAu alloy nanoparticle can be rationally controlled by simply changing the gas atmosphere during the heat treatment.

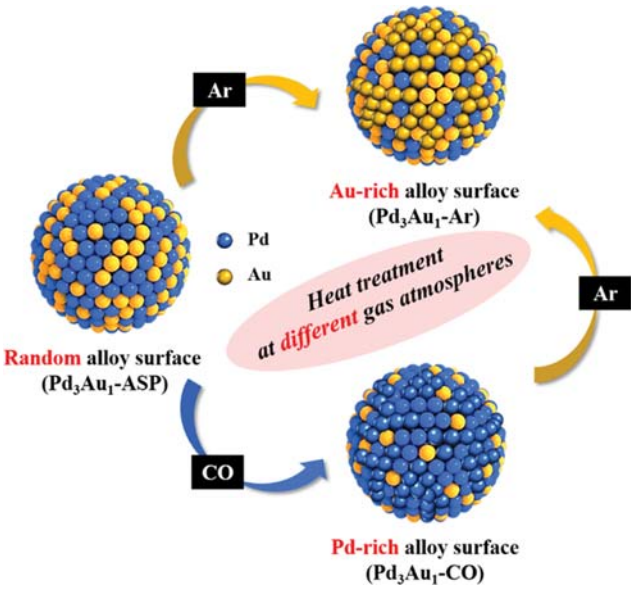

Fig. 1. Schematic representation for the Pd and Au surface segregation in Pd_3Au_1 catalyst by heat treatment using different gas species.

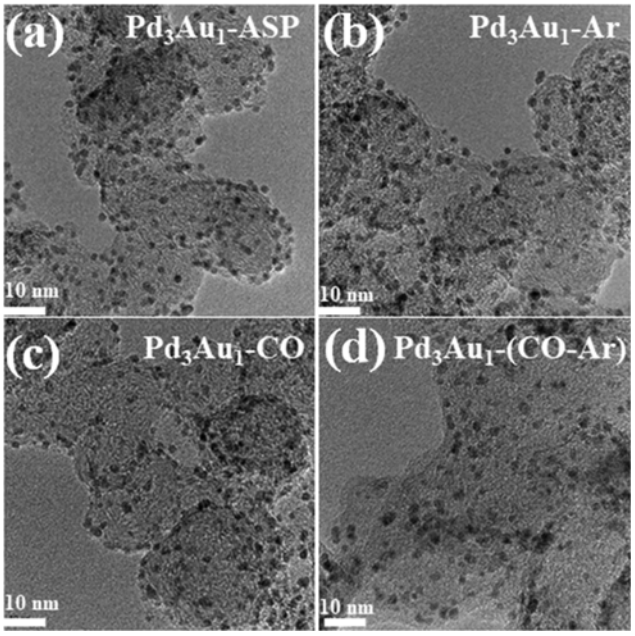

Fig. 2. Transmission electron microscopy (TEM) images of 20 wt% Pd_3Au_1/C electrocatalysts annealed under different gas atmospheres: (a) Pd_3Au_1-ASP, (b) Pd_3Au_1-Ar, (c) Pd_3Au_1-CO, (d) Pd_3Au_1-(CO-Ar).

First, the particle size distribution of the as-prepared and heat treated Pd_3Au_1 nanoparticles was estimated from a sample of ~100 nanoparticles in the TEM images (Fig. 2). As a result, the average nanoparticle size was 3.09 ± 0.27 nm, 3.18 ± 0.24 nm, 3.20 ± 0.25 nm, and 3.28 ± 0.21 nm for Pd_3Au_1-ASP, Pd_3Au_1-Ar, Pd_3Au_1-CO, Pd_3Au_1-(CO-Ar), respectively (Fig. S1, see Supporting Information). In comparison with the particle size of Pd_3Au_1-ASP, all the heat-treated catalysts exhibited slightly increase in size (~0.1 nm) due to particle agglomeration and growth. Therefore, based on the TEM analysis, it was difficult to clearly identify the structural difference among the prepared catalysts.

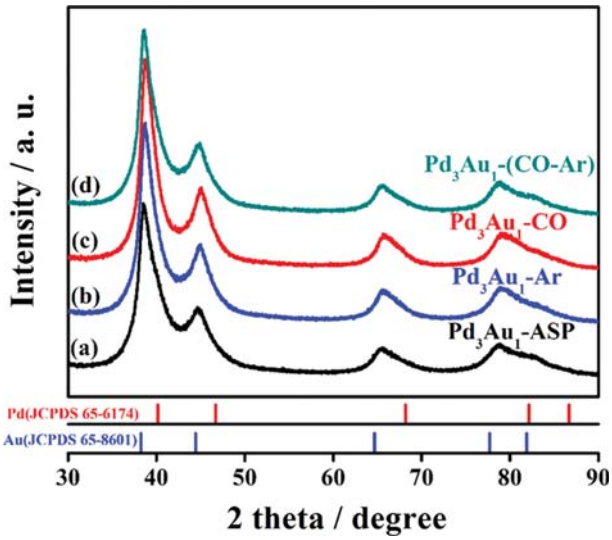

Fig. 3. XRD patterns of Pd_3Au_1 electrocatalysts: (a) Pd_3Au_1-ASP, (b) Pd_3Au_1-Ar, (c) Pd_3Au_1-CO, (d) Pd_3Au_1-(CO-Ar).

To understand the crystal structure of heat-treated Pd_3Au_1 nanoparticles, the XRD analysis was carried out as shown in Fig. 3. Interestingly, all the samples had similar XRD patterns corresponding to face-centered cubic structure, which suggests that the heat-treated electrocatalysts retained the crystal structure even under different gas atmospheres. In comparison with pure Pd (68.17°, JCPDS 65-6174) and Au (64.83°, JCPDS 65-8601), the (220) peaks of Pd_3Au_1 catalysts were found between Pd and Au peaks, which implies the formation of the Pd_3Au_1 alloy [2,10]. In line with the TEM results, the crystallite sizes of Pd_3Au_1-ASP, Pd_3Au_1-Ar, Pd_3Au_1-CO, and Pd_3Au_1-(CO-Ar), were estimated from the (220) diffraction peaks using Scherrer equation and were found to be 3.0, 3.1, 3.2, and 3.3 nm, respectively [30].

In addition, the chemical state and electronic structure of the catalysts were analyzed by XPS (Fig. S2 and Table S1, see Supporting Information). The binding energy of Pd 3d (335.8 eV) and Au 4f (84.0 eV) of all Pd_3Au_1 catalysts was similar and showed a slight shift to lower binding energy in comparison with commercial Pd/C (336.9 eV) and Au/C (84.4 eV), which further proves the Pd_3Au_1 alloy formation in accordance with previous reports [2,10,31]. XPS is a powerful tool to observe the surface composition of our Pd_3Au_1 catalysts; however, X-rays might reach from surface to core part, resulting in bulk scale estimation rather than surface composition. Therefore, the surface composition of Pd_3Au_1 electrocatalysts was exclusively determined by electrochemical methods.

The electrochemical behavior of as-prepared and heat treated Pd_3Au_1 catalysts was investigated by recording cyclic voltammograms (CVs) measured in 0.1 M $HClO_4$ (Fig. 4(a)). Furthermore, the CV of commercial Pd/C (premetek) was compared to evaluate Pd_3Au_1 catalysts relatively. In addition, the Pd surface area ratios of the Pd-based catalysts were calculated by relative comparison based

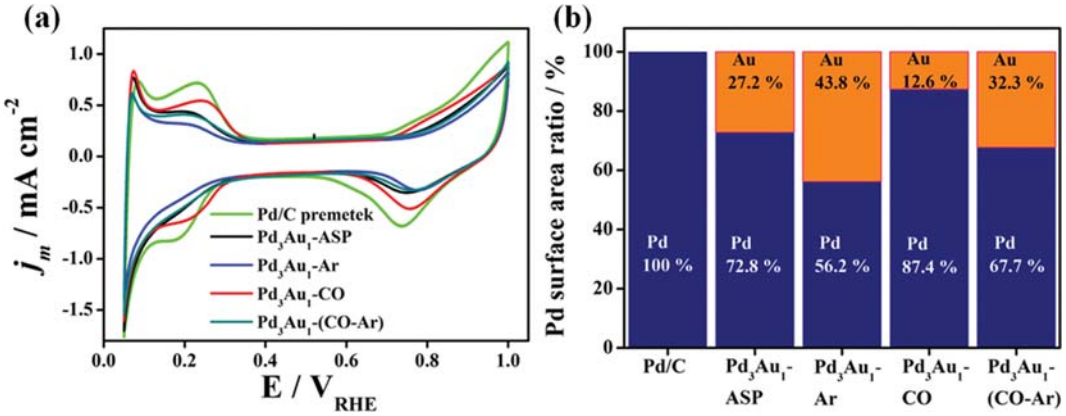

Fig. 4. (a) Cyclic voltammograms (CVs) of Pd_3Au_1 catalysts measured in 0.1 M $HClO_4$, (b) Pd surface area ratio estimated from the CVs. In the figures, the data of commercial Pd/C catalyst were compared with those of Pd_3Au_1 catalysts.

on the CV area of the commercial Pd/C catalyst between 0.05 V and 0.4 V. As shown in Fig. 4(b), the Pd surface composition of the catalysts in percentage values for Pd/C, Pd_3Au_1-ASP, Pd_3Au_1-Ar, Pd_3Au_1-CO, and Pd_3Au_1-(CO-Ar) were estimated to be 100, 87.4, 72.8, 67.7, and 56.2%, respectively. Pd_3Au_1-Ar sample had lower Pd surface ratio compared to Pd_3Au_1-ASP, resulting in the Au-rich surface formation due to the low surface energy of Au. In sharp contrast, the CO-treated catalyst (Pd_3Au_1-CO) had the highest Pd surface composition (87.4%) among the Pd_3Au_1 catalysts, which effectively proves that CO gas has the potential to induce the maximum amount of Pd surface segregation due to strong interaction between Pd and CO while maintaining PdAu alloy structure [10]. Interestingly, in the case of Pd_3Au_1-(CO-Ar) catalyst, it was confirmed that most of the Pd atoms which were segregated to the surface by CO annealing process can be replaced by Au atoms again through the secondary Ar heat treatment.

To thoroughly study the effect of surface rearrangement of Pd_3Au_1 catalysts on the electrochemical properties, ORR polarization curves were obtained as shown in Fig. 5(a). As a control, commercial Pd/C demonstrated superior ORR activity with the highest half-wave ($E_{1/2}$) potential (0.82 V). Interestingly, among all the Pd_3Au_1 alloy samples, CO-treated Pd_3Au_1 (Pd_3Au_1-CO) catalyst showed excellent ORR performance ($E_{1/2}$= 0.79 V) compared to Pd_3Au_1-ASP ($E_{1/2}$= 0.77 V), Pd_3Au_1-(CO-Ar) ($E_{1/2}$= 0.72 V), and Pd_3Au_1-Ar ($E_{1/2}$= 0.71 V). However, for Pd_3Au_1-(CO-Ar) sample, the ORR activity was much lower than Pd_3Au_1-CO but similar to Pd_3Au_1-Ar. Significant changes in the ORR performance of the catalysts can be explained rationally by the following reasons. In general, heat treatment of metal nanoparticles under specific gas atmosphere such as CO is expected to induce surface rearrangements due to the interaction of metal atoms with adsorbates. In our case, during the heat treatment by CO gas, Au atoms are exchanged by Pd atoms at the surface due to high CO binding energy of Pd, resulting in Pd-rich surface [10,28,32]. On the other hand, for Pd_3Au_1-(CO-Ar), the deactivation of Pd_3Au_1 nanoparticles is attributed to the enrichment of inactive Au atoms on the surface after the secondary Ar heat treatment.

As shown in Fig. 5(b), the correlation between half-wave potentials obtained from the ORR polarization curves and Pd surface area ratios calculated from the CVs was plotted for Pd-based electrocatalysts with different surface compositions. As a result, it was clearly proved that the half-wave ($E_{1/2}$) potentials for the ORR changed depending on the Pd surface area ratio and were strongly affected by the number of exposed Pd atoms on the surface. Consequently, the present work provides a facile strategy to change the surface composition of metal alloy nanoparticles. By simply con-

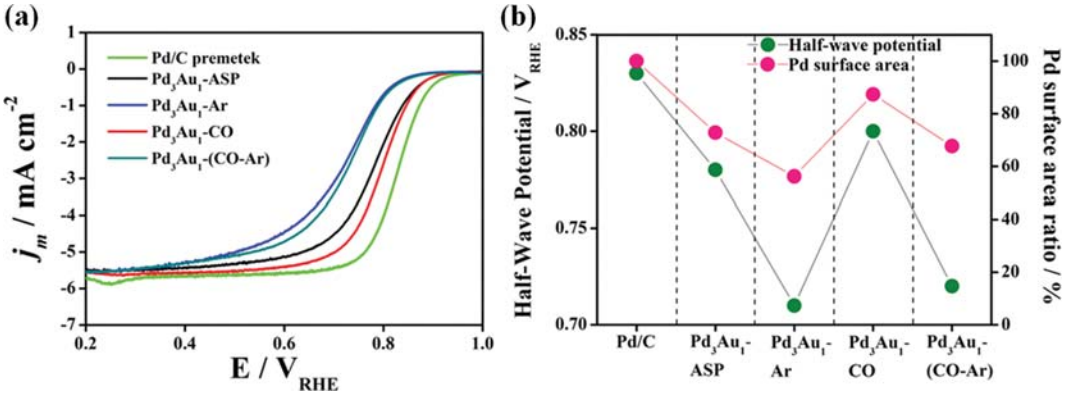

Fig. 5. (a) ORR polarization curves and (b) correlation between their half-wave potentials and Pd surface areas of Pd_3Au_1 catalysts. In the figures, the data of commercial Pd/C catalyst were compared with those of Pd_3Au_1 catalysts.

trolling the gas atmosphere during annealing process, one might be able to find the best surface composition of metal alloy nanoparticles for a certain application.

CONCLUSION

A simple method to control the surface composition in Pd_3Au_1/C catalyst under different gas atmospheres was successfully developed. When CO was used as an annealing gas, CO-induced surface segregation of Pd was generated in Pd_3Au_1 alloy nanoparticles, which resulted in a significant increase in the number of Pd atoms. In contrast, the secondary Ar heat treatment after CO annealing process made Pd_3Au_1 alloy nanoparticles have Au-rich surfaces again. Depending on the number of surface Pd atoms on Pd_3Au_1 alloy nanoparticles, the ORR performance totally changed, and Pd_3Au_1 alloy with the highest Pd surface area showed superior catalytic activity than others. The results clearly confirmed that high CO binding energy of Pd can promote the surface segregation of Pd and exchange the surface Au with Pd atoms positioned at the sub-surface layer. Therefore, the CO-induced surface segregation method is expected to be applied to the development of metal-based alloys with optimum structures and surface compositions for various applications.

ACKNOWLEDGEMENTS

This work was supported by Chungnam National University (2019-2020) and the National Research Foundation of Korea (NRF) grant funded by the Korean government (MSIP) (No. 2018R1C1B6007453, 2018M1A2A2061991, 2018M1A2A2061975).

SUPPORTING INFORMATION

Additional information as noted in the text. This information is available via the Internet at http://www.springer.com/chemistry/journal/11814.

REFERENCES

1. N. M. Markovic, T. J. Schmidt, V. Stamenkovic and P. N. Ross, *Fuel Cells*, **1**, 105 (2001).
2. S.-Y. Lee, N. Jung, D. Y. Shin, H.-Y. Park, D. Ahn, H.-J. Kim, J. H. Jang, D.-H. Lim and S. J. Yoo, *Appl. Catal. B Environ.*, **206**, 666 (2017).
3. M. Sharma, N. Jung and S. J. Yoo, *Chem. Mater.*, **30**, 2 (2018).
4. H. A. Gasteiger, S. S. Kocha, B. Sompalli and F. T. Wagner, *Appl. Catal. B Environ.*, **56**, 9 (2005).
5. H. Sung, M. Sharma, J. Jang, S.-Y. Lee, M.-G. Choi, K. Lee and N. Jung, *Nanoscale*, **11**, 5038 (2019).
6. M. Sharma, J.-H. Jang, D. Y. Shin, J. A. Kwon, D.-H. Lim, D. Choi, H. Sung, J. Jang, S.-Y. Lee, K. Y. Lee, H.-Y. Park, N. Jung and S. J. Yoo, *Energy Environ. Sci.*, **12**, 2200 (2019).
7. H. Erikson, A. Sarapuu, K. Tammeveski, S.-G. Jose and J. M. Feliu, *Electrochem. Commun.*, **13**, 734 (2011).
8. N. Arjona, M. Guerra-Balcázar, L. Ortiz-Frade, G. Osorio-Monreal, L. Álvarez-Contreras, J. Ledesma-Garcíab and L. G. Arriaga, *J. Mater. Chem. A*, **1**, 15524 (2013).
9. L. Zhang, Q. Chang, H. Chen and M. Shao, *Nano Energy*, **29**, 198 (2016).
10. S.-Y. Lee, N. Jung, J. Cho, H.-Y. Park, J. Ryu, I. Jang, H.-J. Kim, E. Cho, Y.-H. Park, H. C. Ham, J. H. Jang and S. J. Yoo, *ACS Catal.*, **4**, 2402 (2014).
11. S. Han, G. Chae and J. S. Lee, *Korean J. Chem. Eng.*, **33**, 1799 (2016).
12. Z. Liu, G. Fu, J. Li, Z. Liu, L. Xu, D. Sun and Y. Tang, *Nano Res.*, **11**, 4686 (2018).
13. G. Ramos-Sánchez, H. Yee-Madeira and O. Solorza-Feria, *Int. J. Hydrogen Energy*, **33**, 3596 (2008).
14. H. Ye, Y. Li, J. Chen, J. Sheng, X.-Z. Fu, R. Sun and C.-P. Wong, *J. Mater. Sci.*, **53**, 15871 (2018).
15. F. Gao and D. W. Goodman, *Chem. Soc. Rev.*, **41**, 8009 (2012).
16. P. Liu and J. K. Nørskov, *Phys. Chem. Chem. Phys.*, **3**, 3814 (2001).
17. P. Strasser, S. Koh, T. Anniyev, J. Greeley, K. More, C. Yu, Z. Liu, S. Kaya, D. Nordlund, H. Ogasawara, M. F. Toney and A. Nilsson, *Nat. Chem.*, **2**, 454 (2010).
18. A. K. Singh and Q. Xu, *ChemCatChem.*, **5**, 652 (2013).
19. V. S. Kumar, S. Kummari, K. Y. Goud, M. Satyanarayana and K. V. Gobi, *Int. J. Hydrogen Energy*, **45**, 1018 (2020).
20. L. Y. Chen, N. Chen, Y. Hou, Z. C. Wang, S. H. Lv, T. Fujita, J. H. Jiang, A. Hirata and M. W. Chen, *ACS Catal.*, **3**, 1220 (2013).
21. H. Erikson, A. Sarapuu, J. Kozlova, L. Matisen, V. Sammelselg and K. Tammeveski, *Electrocatalysis*, **6**, 77 (2015).
22. W. Yan, Z. Tang, L. Wang, Q. Wang, H. Yang and S. Chen, *Int. J. Hydrogen Energy*, **45**, 1018 (2020).
23. P. Paalanen, B. M. Weckhuysen and M. Sankar, *Catal. Sci. Technol.*, **3**, 2869 (2013).
24. Z. Yin, M. Chi, Q. Zhu, D. Ma, J. Sun and X. Bao, *J. Mater. Chem. A*, **1**, 9157 (2013).
25. W. Jiao, C. Chen, W. You, G. Chen, S. Xue, J. Zhang, J. Liu, Y. Feng, P. Wang, Y. Wang, H. Wen and R. Che, *Appl. Catal. B Environ.*, **262**, 118298 (2020).
26. V. K. Kumikov and Kh. B. Khokonov, *J. Appl. Phys.*, **54**, 1346 (1983).
27. L. Z. Mezey and J. Giber, *Appl. Phys. A: Solids Surf.*, **35**, 87 (1984).
28. J. Zhang, H. Jin, M. B. Sullivan, F. C. H. Lim and P. Wu, *Phys. Chem. Chem. Phys.*, **11**, 1441 (2009).
29. J. Greeley and M. Mavrikakis, *Catal. Today*, **111**, 52 (2006).
30. A. Patterson, *Phys. Rev.*, **56**, 978 (1939).
31. P. A. P. Nascente, S. G. C. De castro, R. Landers and G. G. Kleiman, *Phys. Rev. B*, **43**, 4659 (1991).
32. N. Hoshi, K. Kida, M. Nakamura, M. Nakada and K. Osada, *J. Phys. Chem. B*, **110**, 12480 (2006).

Supporting Information

Surface engineering of Pd-based nanoparticles by gas treatment for oxygen reduction reaction

A. Anto Jeffery[*,‡], Sang-Young Lee[,‡], Jiho Min[*], Youngjin Kim[*], Seunghyun Lee[*], Jin Hee Lee[***], Namgee Jung[*,†], and Sung Jong Yoo[****,*****,******,†]**

*Graduate School of Energy Science and Technology (GEST), Chungnam National University, 99 Daehak-ro, Yuseong-gu, Daejeon 34134, Korea
**The Environment Technology Institute, Research Division, Coway R&D Center, 1 Guanak-ro, Gwanak-gu, Seoul 08826, Korea
***Center for Environment & Sustainable Resources, Korea Research Institute of Chemical Technology, Daejeon 34114, Korea
****Center for Hydrogen·Fuel Cell Research, Korea Institute of Science and Technology (KIST), Seoul 02792, Korea
*****Division of Energy & Environment Technology, KIST School, University of Science and Technology (UST), Seoul 02792, Korea
******KHU-KIST Department of Converging Science and Technology, Kyung Hee University, Seoul 02447, Korea
(*Received 15 March 2020 • Revised 10 May 2020 • Accepted 20 May 2020*)

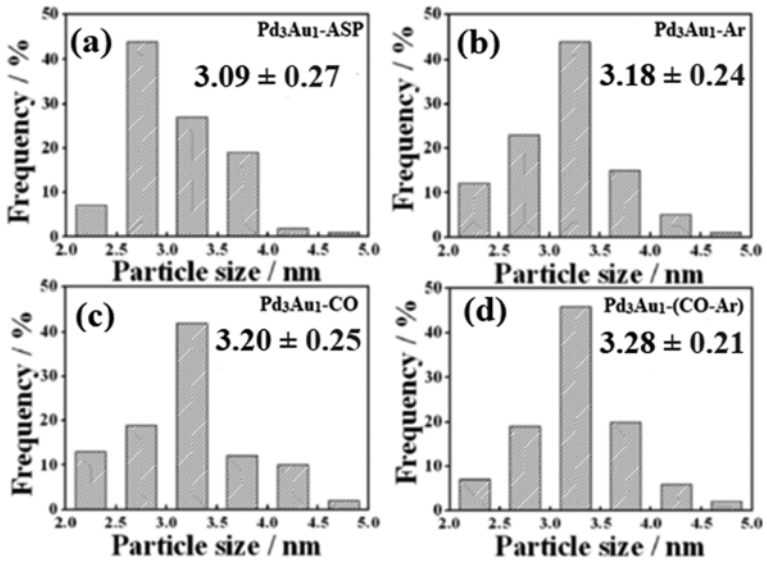

Fig. S1. Particle size distribution histograms of Pd_3Au_1 catalysts: (a) Pd_3Au_1-ASP, (b) Pd_3Au_1-Ar, (c) Pd_3Au_1-CO, and (d) Pd_3Au_1-(CO-Ar).

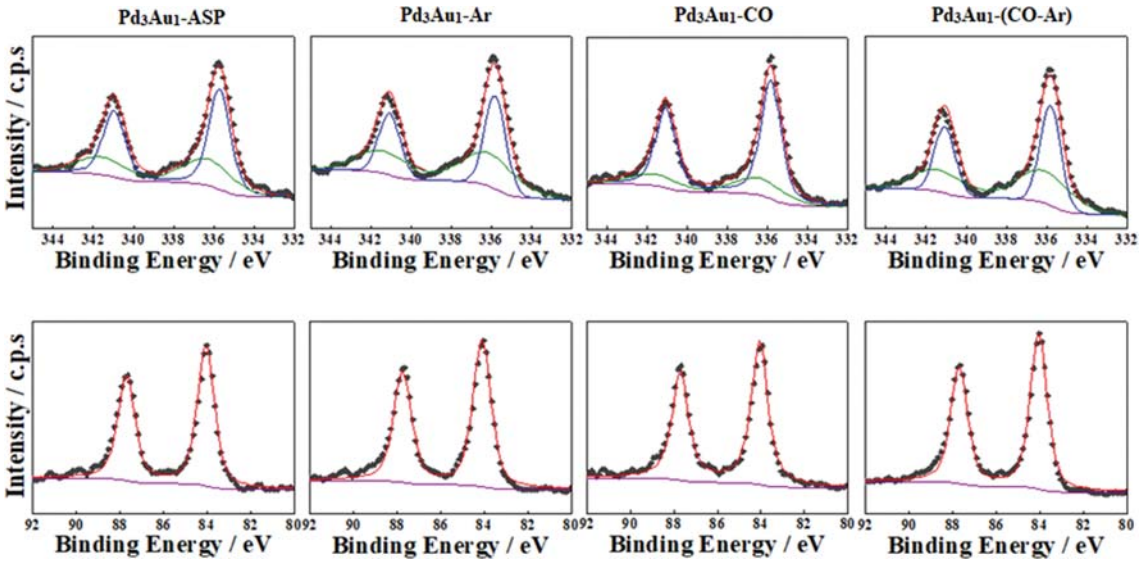

Fig. S2. Pd 3d (top) and Au 4f (bottom) core-level XPS spectra of Pd_3Au_1-ASP, Pd_3Au_1-Ar, Pd_3Au_1-CO, and Pd_3Au_1-(CO-Ar).

Table S1. Summary of XPS measurement data

Samples	Pd 3d			Au 4f		
	Oxidation state	BE (eV)	Relative intensity (%)	Oxidation state	BE (eV)	Relative intensity (%)
Pd_3Au_1-ASP	Pd(0)	335.71	65.4	Au(0)	84.06	-
	Pd(II)	336.18	34.6			
Pd_3Au_1-Ar	Pd(0)	335.81	54.4	Au(0)	84.10	-
	Pd(II)	336.29	45.6			
Pd_3Au_1-CO	Pd(0)	335.82	80.6	Au(0)	84.05	-
	Pd(II)	336.62	19.4			
Pd_3Au_1-(CO-Ar)	Pd(0)	335.81	66.5	Au(0)	84.05	-
	Pd(II)	336.36	33.5			